IEEE Access
Multidisciplinary | Rapid Review | Open Access Journal

Received May 26, 2019, accepted June 11, 2019, date of publication June 21, 2019, date of current version September 17, 2019.

Digital Object Identifier 10.1109/ACCESS.2019.2924194

Tunable Microwave Bandpass Filters With Complementary Split Ring Resonator and Liquid Crystal Materials

DI JIANG[1], YUPENG LIU[1], XIAOYU LI[1], GUOFU WANG[2], AND ZHI ZHENG[1], (Member, IEEE)
[1]School of Information and Communication Engineering, University of Electronic Science and Technology of China, Chengdu 611731, China
[2]School of Electrical and Information Engineering, Guangxi University of Technology, Liuzhou 545006, China

Corresponding author: Xiaoyu Li (uestclixiaoyu@163.com)

This work was supported in part by the National Natural Science Foundation of China under Grant 61871086 and Grant 61761009, and in part by the International Co-Operation Support Plan of Sichuan Province under Grant 2018HH0155.

ABSTRACT In this paper, a novel planar waveguide filter based on liquid crystal materials is devised, and a half-mode corrugated substrate integrated waveguide (HMCSIW) tunable bandpass filter with complementary split ring resonator (CSRR) structure is proposed. The HMCSIW uses an array of quarter-wave open-circuit stubs to replace conventional substrate integrated waveguide (SIW). While retaining the original cut-off frequency of corrugated substrate integrated waveguide (CSIW), we reduce the circuit size by splitting the central axis to achieve the miniaturization. By utilizing band-stop features of the CSRR in microstrip structure and combining with the electronically controlled dielectric constant of liquid crystal materials with high modulation efficiency of inverted microstrip line structure, a CSRR-loaded HMCSIW bandpass filter with liquid crystal materials is implemented. The experimental results demonstrate that the center frequency of the new filter can be adjusted in a range of 0.65 GHz, the pass-band insertion loss is less than 3.4 dB, the return loss is less than -10 dB, and the structure size is 32 mm×76 mm, which verify that the designed tunable band-pass filter achieves good frequency selection performance.

INDEX TERMS Tunable band-pass filter, half-mode corrugated substrate integrated waveguide (HMCSIW), complementary split ring resonator (CSRR), liquid crystal.

I. INTRODUCTION

With increasing demand for wireless communication systems and gradually complex space communication environment, microwave filters should be high performance, miniaturization and easy integration. If the filter index can be adjusted according to user requirements, the cost increase of replacing the device can be avoided and more flexible design ideas can be adopted for entire RF front-end module. It is thus urgent to develop effective tunable filter design methods.

Corrugated substrate integrated waveguide (CSIW) [1], [2] provides a new transmission structure for highly integrated microwave and millimeter wave circuits and systems. Compared with conventional SIW, CSIW can avoid the problem that when the diameter of the metallic via is too small, it is difficult to ensure the machining accuracy in multi-layer structures. Moreover, when applied to electrically tuned waveguide circuits, the problem of short circuit between metallic via structure and DC bias can be resolved, together with simplified processing and reduced hardware cost [3]–[5]. With the advantages of corrugated substrate integrated waveguide structure, it can be easily combined with the metamaterial theory to realize high-performance microwave passive components [6]. A new hollow structure, complementary split ring resonator (CSRR) [7], [8], has attracted extensive investigations, which can generate an equivalent negative dielectric constant near its resonant frequency to form a steep transmission band gap. Therefore, CSRR can be combined with HMCSIW structures to design new microwave passive components.

In addition, as a voltage-controlled tunable material, liquid crystal can be used in microwave and millimeter wave passive devices such as frequency tunable filters [9]–[11], phase shifters [12]–[14] and reconfigurable antennas [15]–[18].

The associate editor coordinating the review of this manuscript and approving it for publication was Yang Yang.

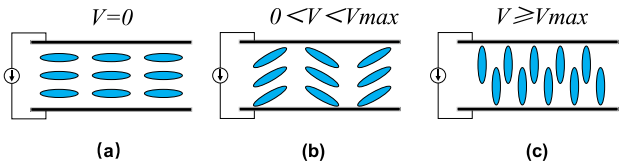

FIGURE 1. The relationship between the orientation vector of liquid crystal molecule and the applied electric field: (a) External voltage V= 0 (b) External voltage 0<V<Vmax (c) External voltage V≥Vmax.

Its advantages include continuous frequency tuning, high tuning linearity, low loss, low working voltage, light weight, small size, and easy preparation [19].

In order to further enhance the adaptability of microwave and millimeter wave passive devices for miniaturization and multi-functional wireless communication systems, a novel planar waveguide filter is designed in this paper with liquid crystal materials, together with HMCSIW tunable bandpass filter and CSRR.

II. DESIGN OF THE LC-BASED HMCSIW-CSRR TUNABLE BANDPASS FILTER

A. LIQUID CRYSTAL

The design of liquid crystal tunable microwave passive devices is mainly based on the principle of liquid crystal electro-optic effect. For liquid crystal cell with aligned liquid crystal molecules, the liquid crystal is used as electro-optic material. When the low-frequency driving voltage is applied outside, the induced electric dipole moment of liquid crystal molecule (the long axis of liquid crystal molecules) interacts with the electric field to produce the moment that drives the direction of liquid crystal director to be consistent with the direction of external electric field, thus changing the distribution of liquid crystal director in space. The type of liquid crystal involved in this paper is nematic liquid crystal, which is easy to be affected by external electric field or magnetic field to produce a certain rule of arrangement, and its dielectric property is the basis of various photoelectric applications.

As shown in Fig. 1, when the applied voltage is 0V, the alignment direction of the liquid crystal molecule's directional vector is parallel to the surface of the cell (the surface of the cell has been oriented). As the applied voltage increases, the directional vector of the liquid crystal molecule will rotate towards the electric field direction gradually. When the applied voltage reaches a certain value (saturation voltage V_{max}), the alignment direction of the long axis of the liquid crystal molecule is parallel to the electric field direction and perpendicular to the cell surface.

Due to the change of refractive index of liquid crystal in the process of applied bias, the effective optical dielectric constant will change gradually, resulting in dielectric anisotropy. Compared with the microstrip resonator with a specific wavelength, when the liquid crystal is used as its dielectric substrate, the resonant frequency of the resonator responds to the changes in the effective dielectric constant of the liquid crystal, so the central frequency tuning characteristic of the filter can be realized.

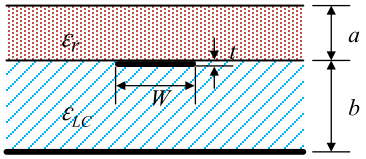

FIGURE 2. Structural sketch of inverted microstrip line.

Generally, the dielectric parameters of liquid crystal vary significantly with the frequency [20]. Normally, the dielectric constant perpendicular to the long axis direction of the molecule is set to $\varepsilon_{\perp}$, and the dielectric constant parallel to the long axis direction of the molecule is $\boldsymbol{\varepsilon}_{//}$, and the dielectric anisotropy can be expressed as [21]:

$$\Delta\varepsilon = \varepsilon_{//} - \varepsilon_{\perp}. \tag{1}$$

It measures the absolute tuning ability of liquid crystal. The relative dielectric anisotropy of the relative tuning ability of liquid crystal is as follows:

$$\eta = \frac{\Delta\varepsilon}{\varepsilon_{//}}. \tag{2}$$

Therefore, the larger the dielectric anisotropy $\Delta\varepsilon$ and relative dielectric anisotropy η are, the wider frequency tuning range can be obtained [22].

Due to the liquid crystal materials' flowing characteristics at room temperature, the plane transmission circuit in this paper is implemented by the inverted microstrip line structure shown in Fig. 2, where the efficiency of the electric field on the liquid crystal has been considered. It is easy to process the inverted microstrip line and connect with other microwave circuits. It can realize the direct and effective contact between liquid crystal and resonant circuit, so as to achieve higher modulation efficiency for liquid crystal. The circuit is placed upside down in space on the lower surface of the upper dielectric substrate, and the electromagnetic field is mostly concentrated in the liquid crystal material. The effective dielectric constant ε_e of the circuit can be expressed as [23]

$$\varepsilon_e = \left[\varepsilon_{LC} + \frac{a}{b}\left(a_1 - b_1 \ln\frac{W}{b}\right)\left(\sqrt{\varepsilon_r} - 1\right)\right]^2 \tag{3}$$

where

$$a_1 = \left(0.5173 - 0.1515 \ln\frac{a}{b}\right)^2 \tag{4}$$

$$b_1 = \left(0.3092 - 0.1047 \ln\frac{a}{b}\right)^2. \tag{5}$$

In the above formulas, "a" is the thickness of the upper dielectric layer, "b" is the thickness of the liquid crystal layer, "W" is the width of the inverted microstrip line, "t" is the thickness of the inverted microstrip line, and "εr" is the dielectric constant of the upper dielectric layer.

If t/b<<1, the characteristic impedance of the inverted microstrip line can be obtained by the least squares curve

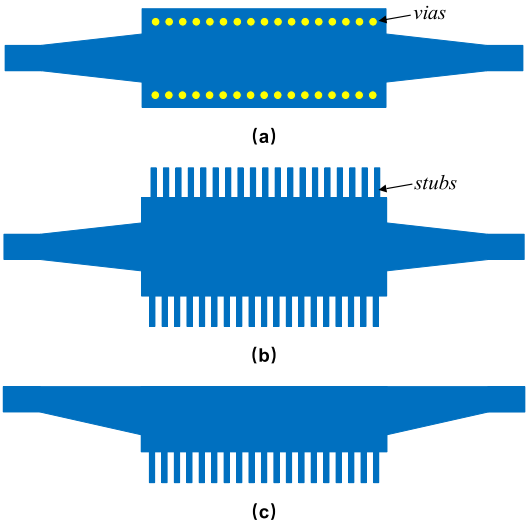

FIGURE 3. Comparison of the SIW, CSIW and HMCSIW structure fed by microstrips: (a) SIW (b) CSIW (c) HMCISW.

fitting method [23]:

$$z_0 = \frac{60}{\sqrt{\varepsilon_e}} \ln\left[\frac{f(u)}{u} + \sqrt{1+\left(\frac{2}{u}\right)^2}\right] \tag{6}$$

$$f(u) = 6 + (2\pi - 6)\exp\left[-\left(\frac{30.666}{u}\right)^{0.7528}\right] \tag{7}$$

$$u = \frac{W}{b} \tag{8}$$

In this structure, the transmission circuit and the liquid crystal are placed between the bottom metal and the upper dielectric substrate, while ensuring that the liquid crystal does not overflow, so as to achieve the packaging requirement of liquid crystal microwave devices.

B. HMCSIW PLANAR WAVEGUIDE AND CSRR RESONANT STRUCTURE

The CSIW uses quarter wavelength open circuit stubs instead of the traditional metallized grounding vias of SIW, which can realize waveguide mode propagation similar to SIW in a specific frequency band. In order to achieve bias voltage loading, the liquid crystal tuning circuit needs to form an electric potential difference with the ground, and the metallized via should be avoided in the design. Therefore, the CSIW is suitable for the liquid crystal tuning circuit.

The CSIW structure is illustrated in Fig. 3 (b). The upper and lower parts are the same as the traditional SIW structure and are metal layers, while the left and right sides use quarter wavelength open circuit stubs to replace the metallization vias. According to the waveguide cavity mode, when TE_{10} mode electromagnetic field is propagated in a rectangular waveguide, the axis of the electric field can be equivalent to an ideal magnetic wall. Similarly, the CSIW can also achieve a similar structure as the half-mode substrate integrated waveguide (HMSIW), which can propagate

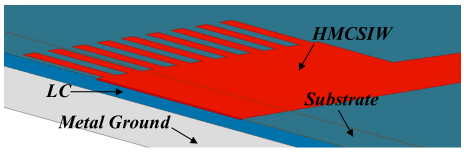

FIGURE 4. Structural sketch of inverted microstrip line in this paper.

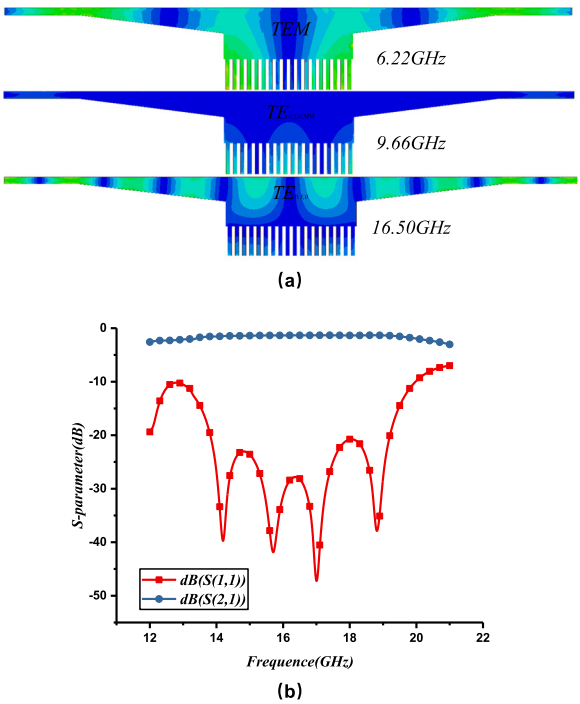

FIGURE 5. (a)The electric field distribution of HMCSIW at 6.22 GHz, 9.66 GHz and 16.5 GHz (b) the frequency response curve of HMCSIW in waveguide mode.

$TE_{0.5,0}$ mode in the main mode of rectangular waveguide by splitting the central axis of full-mode TE_{10} waveguide. The size of the HMCSIW is reduced by nearly half compared with the CSIW under the same structure and technology without affecting the transmission of main mode.

To exploit the HMCSIW propagation characteristics, we the electromagnetic simulation software HFSS to model and simulate it. On both sides of the main waveguide of HMCSIW, a graded line impedance transformation structure is added. The whole model is designed with an inverted microstrip structure as shown in Fig. 4. The upper dielectric substrate is Rogers RT/duroid 5880 (tm) substrate with a thickness of 0.508mm, the liquid crystal layer is 0.254mm, and the thickness of the metal floor is 1mm.

Fig. 5 (a) plots the electric field distribution of the HMCSIW at 6.22 GHz, 9.66 GHz and 16.5 GHz. Similar to the CSIW transmission mode, it can realize TEM, $TE_{0.5,0,MM}$, $TE_{0.5,0}$ transmission modes, so it can be completely equivalent to CSIW half-mode transmission line. Fig. 5 (b) shows the frequency response curve of the HMCSIW in waveguide mode and we can know that HMCSIW itself has band-pass-like characteristics, which is

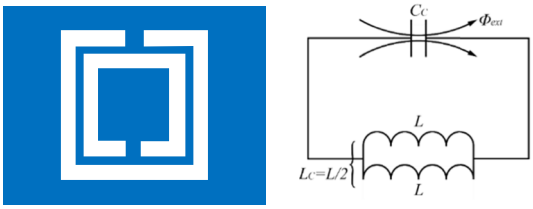

FIGURE 6. The structure of square CSRR (a) CSRR unit (b) the parallel LC equivalent circuit.

consistent with the simulation and test results [24]. The insertion loss is less than 0.7 dB and the return loss is less than -20 dB in the frequency range from 13.82 GHz to 19.20GHz.

The CSRR unit is a complementary structure formed by the position exchange of split ring resonator's (SRR) dielectric material and metal material, and is a resonant unit with stopband characteristic in microstrip structure first proposed by Falcone et al [7].

As shown in Fig. 6, the structure of square CSRR with N = 2 is illustrated. When the excitation perpendicular to the CSRR plane is adopted, the CSRR structure can be equivalent to the LC resonant structure. The induced current flows on the strip metal connecting the inner ring and outer ring to form inductance, and the gap between strip metals will form capacitance, and the CSRR structure will produce electric resonance.

As depicted in Fig. 6, the parallel LC equivalent circuit of the CSRR unit has a dual relationship with the equivalent circuit of SRR. Based on the mutual coupling theorem, the relationship between the CSRR and capacitance and inductance of the SRR can be modeled as follows [25]:

$$C_c = \frac{4\varepsilon_0 L_s}{\mu_0} \tag{9}$$

$$C_0 = \frac{4\varepsilon_0 L_0}{\mu_0} \tag{10}$$

In the formulas (9) and (10), L_s is the equivalent inductance, C_0 is the equivalent capacitance between two square rings in SRR structure, L_0 is the equivalent inductance, and C_c is the equivalent capacitance in CSRR structure. The constants of ε_0, μ_0 are dielectric constant and permeability in vacuum, respectively. The resonant frequency of CSRR is given by

$$f_0 = \frac{1}{2\pi\sqrt{L_c C_c}} = \frac{1}{2\pi\sqrt{(L_0/4)\, C_c}} \tag{11}$$

When multiple CSRRs are cascaded, the resonant frequency will not change, but the ability to suppress the signal in stopband will be enhanced. Because the upper and lower surfaces of the HMCSIW structure are covered with a metal layer, it is easy to etch CSRR resonant ring. When the resonant frequency of the CSRR is less than the HMCSIW cut-off frequency, the HMCSIW structure can produce a passband by loading the CSRR, which can be applied in designing the HMCSIW filter.

C. FILTER CONFIGURATION

Based on the above discussion, the CSRR resonant ring is loaded on the HMCSIW, and liquid crystal is used as the internal dielectric material of the HMCSIW to realize the adjustable bandpass filter. By changing the size and position of the CSRR structures and utilizing the coupling effect between the inner and outer rings on the transmission characteristics of the HMCSIW, the required central frequency and bandwidth are obtained. The central frequency of the filter is tuned by changing the dielectric anisotropy of the liquid crystal through bias voltage.

In this design, for HMCSIW transmission lines, the main factors affecting their transmission characteristics are the width of the main waveguide "W1" and the length of the open-circuit stubs "ls". This width should make the corresponding cut-off frequency outside the bandwidth of the designed filter, so as to ensure that the filter's passband response will not be cut off by the HMCSIW. The length of microstrip open subs "ls" is approximately equal to a quarter of the waveguide wavelength at the center frequency. The width "ws" and spacing "p" of corrugated microstrip lines are similar to the diameter and spacing of metal vias in HMSIW [26].

For the characteristics of a single CSRR unit, the axial electric field excitation is adopted in the simulation analysis. The commonly used empirical formula for calculating the size of CSRR structure is that the circumference of CSRR structure is about half wavelength corresponding to the resonance frequency.

$$L_{total} \approx \frac{\lambda}{2} = \frac{c}{2f\sqrt{\varepsilon_{eff}}} \tag{12}$$

where c is the speed of light, L_{total} is the total length of CSRR and ε_{eff} is the effective dielectric constant, so the initial outer edge length of square CSRR is rt1= L_{total}/4. The CSRR structure shown in Fig. 6(a) is put into the rectangular cavity to excite the electric field vertically through the torus. We studied the influence of the radius of the outer ring, the distance between the inner ring and the outer ring and the distance between the openings on the resonance frequency of CSRR in Fig. 7. According to formula (11), when the outer ring length increases, the capacitance increases and the resonance frequency decreases. It can be seen that the CSRR produces obvious transmission stopband at 17.2 GHz (rt1=3mm). When other parameters remain unchanged, the CSRR resonant frequency will increase with the increase of ring spacing and opening spacing.

Fig. 8 shows the HMCSIW structure loaded with a single CSRR resonant unit, and the specific parameters are annotated in Table 1. The HMCSIW structure transits to 50Ω microstrip line at both ends through gradient impedance transform structure. To meet the transition requirements of microstrip and inverted microstrip structure in wide band, overlapping splicing between upper and lower circuits is adopted to ensure that the modulation voltage is added to the liquid crystal layer, and coplanar waveguide structure is

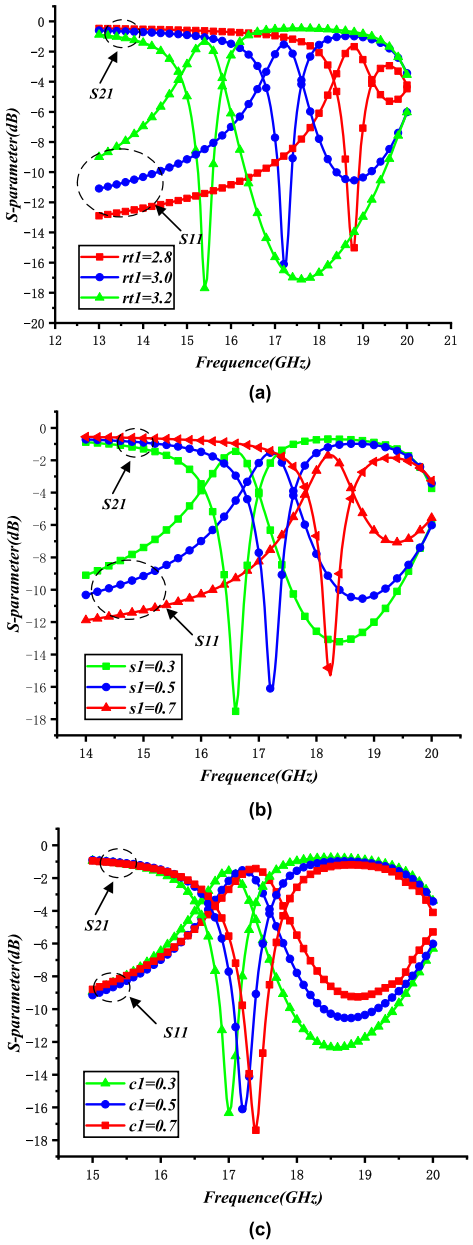

FIGURE 7. The influence of main parameters on CSRR resonance characteristics (a) rt1(b)s1 (c)c1.

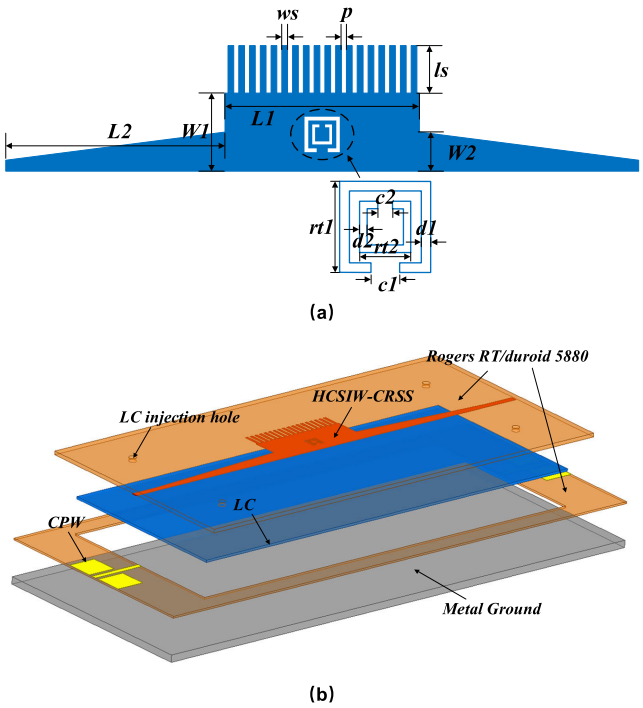

FIGURE 8. (a)The HMCSIW structure loaded with a single CSRR resonant ring (b) overall structure.

TABLE 1. Geometrical parameters of the designed tunable LC-based bandpass filter (unit: mm).

Parameters	*Value*	*Parameters*	*Value*
L1	*13*	*d1*	*0.15*
L2	*15*	*d2*	*0.15*
W1	*5.37*	*d3*	*0.2*
W2	*2.66*	*d4*	*0.15*
ls	*3.2*	*d5*	*0.15*
ws	*0.37*	*d6*	*0.1*
p	*0.35*	*c1*	*0.7*
rt1	*3*	*c2*	*0.3*
rt2	*2*	*c3*	*0.3*
rt3	*1.85*	*c4*	*0.5*
rt4	*1.1*	*c5*	*0.35*
rt5	*1.96*	*c6*	*0.3*
rt6	*1.34*	*s*	*1.1*

adopted at the input feed port. The thickness of the upper Rogers RT/duroid 5880 (tm) substrate is 0.508 mm and the lower layer is 0.254 mm. The thickness of the liquid crystal layer is 0.254 mm, the reference range of dielectric constant is 2.4-2.8, and the area of the liquid crystal part is 26 mm $\times$ 65 mm.

By loading the transmission stopband introduced by CSRR, the simulation results of transmission response of HMCSIW transmission line loaded with a single CSRR structure are given in Figure 9. It is noticed that there is a transmission zero in the upper band, and an out-of-band suppression larger than 18 dB.

In order to obtain better band-pass characteristics, we introduce two CSRRs to construct two transmission zeros. By adjusting the dimensions of the two CSRRs, the resonant points with stopband characteristics are located at both sides of the HMCSIW class band-pass characteristics, thus forming a band-pass filter and increasing out-band suppression. The final CSRR size and the distance between two rings can be optimized by the electromagnetic simulation software HFSS.

Fig. 10 shows the simulation results of the transmission response of the structure in the HFSS software. There is a transmission zero in each side band of the passband, which increases the out-of-band suppression, and the out-of-band suppression can reach 32 dB. The center frequency of the filter ranges from 16.32 GHz to 17.52 GHz to achieve 1.2 GHz shift. The 3dB bandwidth is larger than 2.56 GHz. The return loss |S11| is greater than 15dB. At the extreme point, the insertion loss of |S21| is greater than 20dB and the insertion loss of |S21| is less than 1dB.

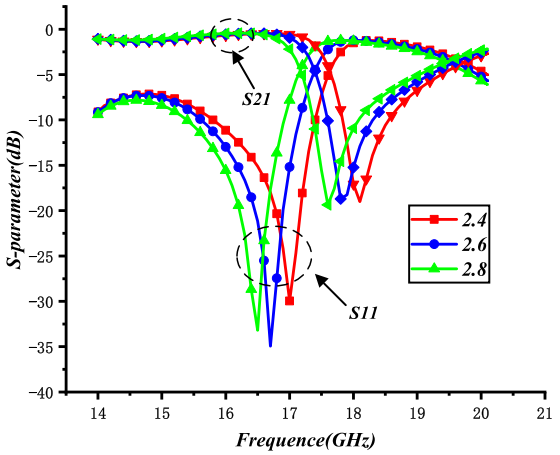

FIGURE 9. The simulation results of the transmission response of the structure.

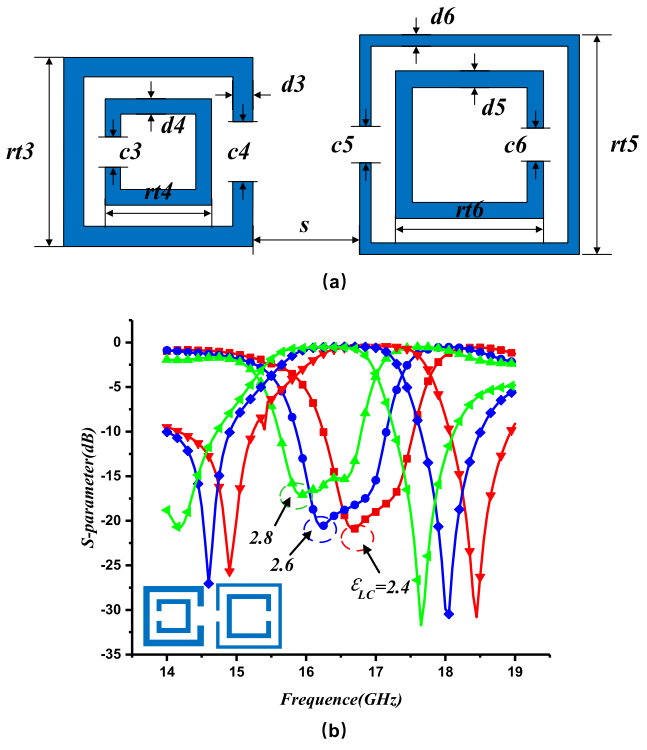

FIGURE 10. The transmission response (a) two CSRR resonant units (parameters are given in table 1) (b) simulation results of transmission response of two resonant units.

III. EXPERIMENTAL RESULTS AND DISCUSSION

To verify design feasibility of the filter, the filter was processed and tested according to the structure size shown in Fig. 11. The polyimide was uniformly rotated on the back of the dielectric substrate and on the front of the metal substrate by friction orientation method, thus realizing orientation localization of liquid crystal molecules. After fixing the screw around the three-layer structure components, the solidified adhesive was applied vertically to form a closed test device. Finally, the liquid crystal material was injected into the liquid crystal cell by a micro-injection plug for testing.

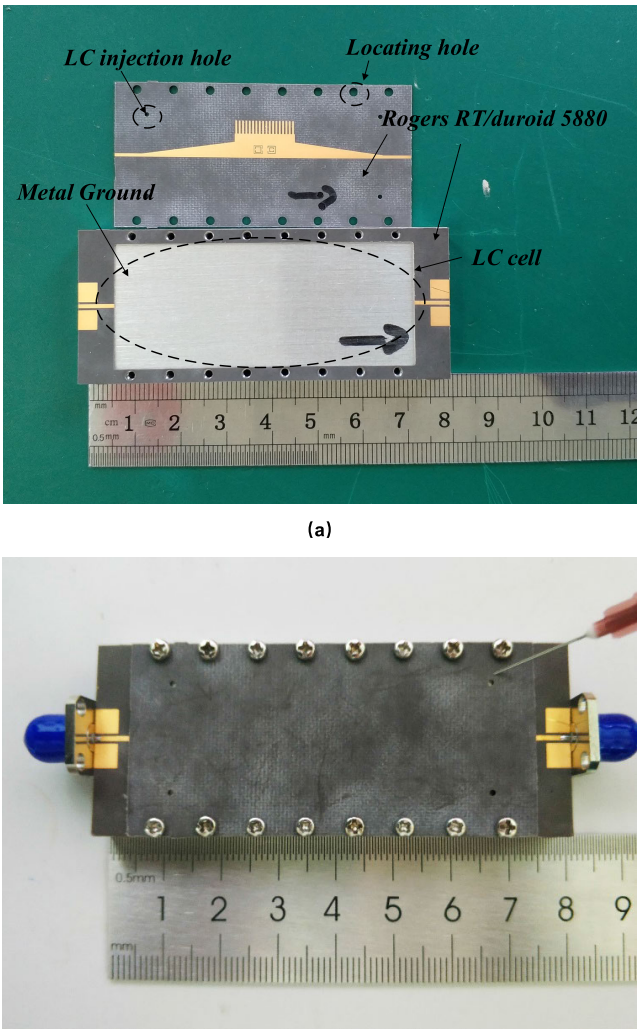

FIGURE 11. Pictures of fabricated device. (a) The back of the substrate; (b) the whole structure of the prototype with LC injection.

In the test system shown in Figure 12, we use the PNA-X vector network analyzer of Keysight Technologies. The vector network has built-in bias-T module, which provides the bias loading port for the vector network. In practical application, in order to prevent the molecule bond of liquid crystal from breaking when the applied electrostatic field is too large, which will cause irreversible damage to the liquid crystal materials, the 1KHz low frequency square wave signal is used instead of the electrostatic field. The function waveform signal generator provides 1KHz low frequency square wave signal modulation voltage (0V-30V), which is loaded onto the device under test through the radio frequency input port.

The measured results given in Fig. 13 show that when the bias voltage varies in the 2V-22V range, the center frequency of the filter shifts from 16.41GHz to 17.06GHz, the bandwidth of the filter is greater than 0.65GHz, the return loss is greater than 10dB, the insertion loss is less than 3.4dB, and the transmission zero point outside the band reaches 18dB. Comparing with the simulation results

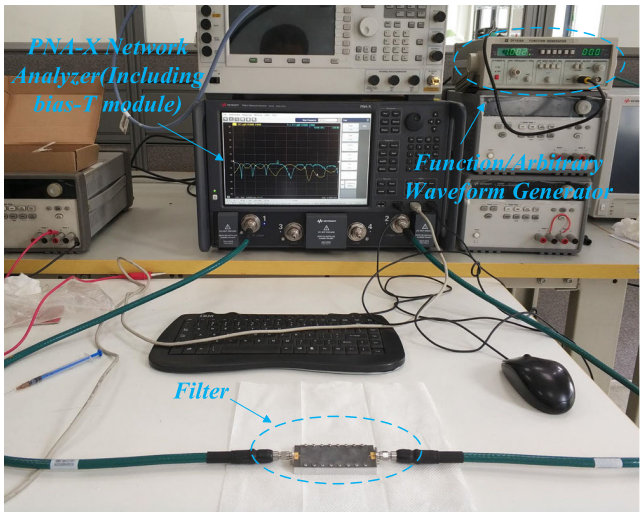

FIGURE 12. Test platform for liquid crystal tunable filter.

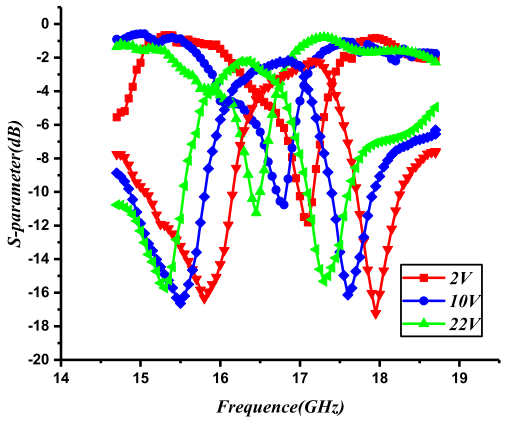

FIGURE 13. The measured results of CSRR-loaded HMCSIW bandpass filter with two resonant units.

given in Fig. 9, it is observed that the center frequency of the filter varies within the bias voltage of 2V-22V. It is seen from Fig. 11 that the liquid crystal starts tuning at the bias voltage of 2V and almost stops at 22V. It means that liquid crystal cells have not been switched when bias voltage is below 2V, while 22V bias voltage fully switches liquid crystal cells. That is, the measurements are well consistent with the simulation results.

IV. CONCLUSION

In this paper, CSRR electromagnetic properties and HMCSIW transmission characteristics of half mode corrugated substrate integrated waveguide were analyzed, and the HMCSIW liquid crystal tunable filter with dynamic frequency selection and good off-band inhibition was designed by combing the electrical dielectric anisotropy of adjustable liquid crystal materials in microwave frequency band. Note that the reasons for the large test results of the filter insertion loss in this work are mainly due to the loss caused by the overlapped splicing structure between the surface microstrip line and the inverted microstrip structure, and the inhomogeneity of liquid crystal leakage during injection and encapsulation. Both simulations and measurements verify the design feasibility, which lays a foundation for future investigation of miniaturized adjustable planar waveguide filters.

REFERENCES

[1] D. G. Chen and K. W. Eccleston, "Substrate integrated waveguide with corrugated wall," in *Proc. Asia–Pacific Microw. Conf.*, Dec. 2008, pp. 1–4.
[2] K. W. Eccleston, "Mode analysis of the corrugated substrate integrated waveguide," *IEEE Trans. Microw. Theory Techn.*, vol. 60, no. 10, pp. 3004–3012, Oct. 2012.
[3] M. Abdolhamidi and M. Shahabadi, "X-band substrate integrated waveguide amplifier," *IEEE Microw. Wireless Compon. Lett.*, vol. 18, no. 12, pp. 815–817, Dec. 2008.
[4] J.-X. Chen, W. Hong, Z.-C. Hao, H. Li, and K. Wu, "Development of a low cost microwave mixer using a broad-band substrate integrated waveguide (SIW) coupler," *IEEE Microw. Wireless Compon. Lett.*, vol. 16, no. 2, pp. 84–86, Feb. 2006.
[5] F. F. He, K. Wu, W. Hong, H. J. Tang, H. B. Zhu, and J. X. Chen, "Suppression of second and third harmonics using λ/4 low-impedance substrate integratedwaveguide bias line in power amplifier," *IEEE Microw. Wireless Compon. Lett.*, vol. 18, no. 7, pp. 479–481, Jul. 2008.
[6] C. Caioz and T. Itoh, *Electromagnetic Metamaterials: Transmission Line Theory and Microwave Applications*. Hoboken, NJ, USA: Wiley, 2006.
[7] F. Falcone, T. Lopetegi, and J. D. Baena, "Effective negative-ε stop-band microstrip lines based on complementary split ring resonators," *IEEE Microw. Wireless Compon. Lett.*, vol. 14, no. 6, pp. 280–282, Jun. 2004.
[8] J. Bonache, F. Martín, F. Falcone, J. D. Baena, T. Lopetegi, J. García-García, M. A. G. Laso, I. Gil, A. Marcotegui, R. Marqués, and M. Sorolla, "Application of complementary split-ring resonators to the design of compact narrow band-pass structures in microstrip technology," *Microw. Opt. Technol. Lett.*, vol. 46, no. 5, pp. 508–512, 2005.
[9] V. Urruchi, C. Marcos, J. Torrecilla, J. M. Sánchez-Pena, and K. Garbat, "Note: Tunable notch filter based on liquid crystal technology for microwave applications," *Rev. Sci. Instrum.*, vol. 84, no. 2, 2013, Art. no. 026102.
[10] A. E. Prasetiadi, O. H. Karabey, C. Weickhmann, T. Franke, W. Hu, M. Jost, M. Nickel, and R. Jakoby, "Continuously tunable substrate integrated waveguide bandpass filter in liquid crystal technology with magnetic biasing," *Electron. Lett.*, vol. 51, no. 20, pp. 1584–1585, Oct. 2015.
[11] E. Polat, R. Reese, M. Jost, C. Schuster, M. Nickel, R. Jakoby, and H. Maune, "Tunable liquid crystal filter in nonradiative dielectric waveguide technology at 60 GHz," *IEEE Microw. Wireless Compon. Lett.*, vol. 29, no. 1, pp. 44–46, Jan. 2019.
[12] S. Müller, P. Scheele, C. Weil, C. Weil, M. Wittek, C. Hock, and R. Jakoby, "Tunable passive phase shifter for microwave applications using highly anisotropic liquid crystals," in *IEEE MTT-S Int. Microw. Symp. Dig.*, Jun. 2004, pp. 1153–1156.
[13] Y. Utsumi, T. Kamei, K. Saito, and H. Moritake, "Increasing the speed of microstrip-line-type polymer-dispersed liquid-crystal loaded variable phase shifter," *IEEE Trans. Microw. Theory Techn.*, vol. 53, no. 11, pp. 3345–3353, Nov. 2005.
[14] F. Goelden, A. Gaebler, M. Goebel, A. Manabe, S. Mueller, and R. Jakoby, "Tunable liquid crystal phase shifter for microwave frequencies," *Electron. Lett.*, vol. 45, no. 13, pp. 686–687, Jun. 2009.
[15] O. H. Karabey, S. Bildik, S. Strunck, A. Gaebler, and R. Jakoby, "Continuously polarisation reconfigurable antenna element by using liquid crystal based tunable coupled line," *Electron. Lett.*, vol. 48, no. 3, pp. 141–143, 2012.
[16] O. H. Karabey, A. Gaebler, S. Strunck, and R. Jakoby, "A 2-D electronically steered phased-array antenna with 2×2 elements in LC display technology," *IEEE Trans. Microw. Theory Techn.*, vol. 60, no. 5, pp. 1297–1306, May 2012.
[17] S. Bildik, S. Dieter, C. Fritzsch, W. Menzel, and R. Jakoby, "Reconfigurable folded reflectarray antenna based upon liquid crystal technology," *IEEE Trans. Antennas Propag.*, vol. 63, no. 1, pp. 122–132, Jan. 2015.

[18] G. Xu, H.-L. Peng, C. Sun, J.-G. Lu, Y. P. Zhang, and W.-Y. Yin, "Differential probe fed liquid crystal-based frequency tunable circular ring patch antenna," *IEEE Access*, vol. 6, pp. 3051–3058, 2017.
[19] R. Dickie, P. Baine, R. Cahill, E. Doumanis, G. Goussetis, S. Christie, N. Mitchell, V. Fusco, D. Linton, J. Encinar, R. Dudley, D. Hindley, M. Naftaly, M. Arrebola, and G. Toso, "Electrical characterisation of liquid crystals at millimetre wavelengths using frequency selective surfaces," *Electron. Lett.*, vol. 48, no. 11, pp. 611–612, 2012.
[20] F. Gölden, "Liquid crystal based microwave components with fast response times: Material, technology, power handling capability," Ph.D. dissertation, Dept. Microw. Technol., Technische Universität Darmstadt, Darmstadt, Germany, 2010.
[21] A. Gaebler, F. Goelden, S. Mueller, and R. Jakoby, "Efficiency considerations of tuneable liquid crystal microwave devices," in *Proc. German Microw. Conf.* Hamburg-Harburg, Germany: VDE, 2011, pp. 1–4.
[22] C. Fritzsch and M. Wittek, "Recent developments in liquid crystals for microwave applications," in *Proc. IEEE Int. Symp. Antennas Propag. USNC/URSI Nat. Radio Sci. Meeting*, Jul. 2017, pp. 1217–1218. doi: 10.1109/APUSNCURSINRSM.2017.8072651.
[23] R. S. Tomar and P. Bhartia, "New quasi-static models for the computer-aided design of suspended and inverted microstrip lines (short paper)," *IEEE Trans. Microw. Theory Techn.*, vol. 35, no. 4, pp. 453–457, Apr. 1987.
[24] K. W. Eccleston, "Transmission properties of full-mode and half-mode folded corrugated SIW," in *Proc. Asia–Pacific Microw. Conf.*, Nov. 2014, pp. 43–45.
[25] M. Gil, I. Gil, J. Bonache, J. García-García, and F. Martín, "Metamaterial transmission lines with extreme impedance values," *Microw. Opt. Technol. Lett.*, vol. 48, no. 12, pp. 2499–2506, 2006.
[26] K. Wu, D. Deslandes, and Y. Cassivi, "The substrate integrated circuits—A new concept for high-frequency electronics and optoelectronics," in *Proc. 6th Int. Conf. Telecommun. Mod. Satell., Cable Broadcast. Service*, vol. 1, Oct. 2003, p. P-3.

DI JIANG received the M.S. and Ph.D. degrees in electromagnetic field and microwave technology from the University of Electronic Science and Technology of China (UESTC), Chengdu, China. Since 2014, he has been an Associate Professor in electromagnetic fields and microwave techniques with the School of Information and Communication Engineering, University of Electronic Science and Technology of China. His research interests include high-performance microwave and millimeter-wave reconfigurable devices, antennas, and microwave device modeling, especially in applied liquid crystal materials to the design of microwave and millimeter-wave devices.

YUPENG LIU received the Ph.D. degree in electromagnetic field and microwave technology from the University of Electronic Science and Technology of China (UESTC), Chengdu, China. His current research interests include the tunable RF and microwave passive circuits research, and reconfigurable compact antennas analysis and design.

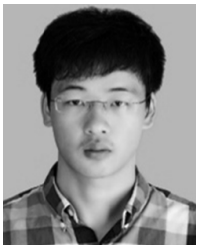

XIAOYU LI is currently pursuing the M.S. degree with the School of Information and Communication Engineering, University of Electronic Science and Technology of China, Chengdu, China. His research interests include liquid crystal technologies and reconfigurable antenna/array.

GUOFU WANG was born in Pingdingshan, China, in 1977. He received the M.S. and Ph.D. degrees in signal and information processing from the Chinese Academy of Sciences, in 2005 and 2007, respectively. Since 2017, he has been a Professor with the School of Electrical and Information Engineering, Guangxi University of Technology. His current research interests include adaptive signal processing and image processing, which have rich research experience in the development of key technologies of photoelectric countermeasure turntable.

ZHI ZHENG (M'11) received the M.S. and Ph.D. degrees in electronic engineering and information and communication engineering from the University of Electronic Science and Technology of China (UESTC), Chengdu, China, in 2007 and 2011, respectively. From 2014 to 2015, he was an Academic Visitor with the Department of Electrical and Electronic Engineering, Imperial College London, U.K. Since 2011, he has been with the School of Information and Communication Engineering, UESTC, where he is currently an Associate Professor. His research interests include statistical and array signal processing, including direction finding, source localization, target tracking, sparse array design, robust adaptive beamforming, jammer suppression, compressive sensing, machine learning, and convex optimization, with applications to radar, sonar, satellite navigation, wireless communications, and wireless sensor networks.